HHS Public Access

Author manuscript

Bioconjug Chem. Author manuscript; available in PMC 2023 October 18.

Published in final edited form as:

Bioconjug Chem. 2023 January 18; 34(1): 193–203. doi:10.1021/acs.bioconjchem.2c00461.

Dynamic Imine Bonding Facilitates Mannan Release from a Nanofibrous Peptide Hydrogel

Brett H. Pogostin,
Department of Bioengineering, Rice University, Houston, Texas 77005, United States

Gabriel Saenz,
Department of Chemistry, Rice University, Houston, Texas 77005, United States

Carson C. Cole,
Department of Chemistry, Rice University, Houston, Texas 77005, United States

Erin M. Euliano,
Department of Bioengineering, Rice University, Houston, Texas 77005, United States

Jeffrey D. Hartgerink,
Department of Bioengineering and Department of Chemistry, Rice University, Houston, Texas 77005, United States

Kevin J. McHugh
Department of Bioengineering and Department of Chemistry, Rice University, Houston, Texas 77005, United States

Abstract

Recently, there has been increased interest in using mannan as an immunomodulatory bioconjugate. Despite notable immunological and functional differences between the reduced (R-Man) and oxidized (O-Man) forms of mannan, little is known about the impact of mannan oxidation state on its *in vivo* persistence or its potential controlled release from biomaterials that may improve immunotherapeutic or prophylactic efficacy. Here, we investigate the impact of oxidation state on the *in vitro* and *in vivo* release of mannan from a biocompatible and immunostimulatory multidomain peptide hydrogel, $K_2(SL)_6K_2$ (abbreviated as K_2), that has been previously used for the controlled release of protein and small molecule payloads. We observed

Corresponding Authors: **Jeffrey D. Hartgerink** – *Department of Bioengineering and Department of Chemistry, Rice University, Houston, Texas 77005, United States*; Phone: +1 (713) 348-4142; jdh@rice.edu; **Kevin J. McHugh** – *Department of Bioengineering and Department of Chemistry, Rice University, Houston, Texas 77005, United States*; Phone: +1 (713) 348-8089; kevin.mchugh@rice.edu.

Supporting Information

The Supporting Information is available free of charge at https://pubs.acs.org/doi/10.1021/acs.bioconjchem.2c00461.
Figure S1: size exclusion chromatography (SEC) of unmodified mannan and R-Man. Figure S2: FTIR of E_2 loaded with O-Man and R-Man. Figure S3: additional negative stain TEM images of R-Man. Figure S4: oscillatory rheology frequency sweeps of mannan-loaded hydrogels. Figure S5: rheological characterization of E_2 loaded with O-Man and R-Man. Figure S6: schematic of custom 3D-printed plate for *in vitro* release assays. Figure S7: *in vitro* release from the E_2 hydrogel. Figure S8: full 56-day fitted *in vivo* release curves. Figure S9: *in vivo* release curve of Gly+O-Man experiment. Figure S10: UPLC and MALDI MS characterization data of the K_2 peptide. Figure S11: UPLC and MALDI MS characterization data of the E_2 peptide. (PDF)

Complete contact information is available at: https://pubs.acs.org/10.1021/acs.bioconjchem.2c00461

The authors declare the following competing financial interest(s): K.J.M. is a paid consultant for Particles for Humanity, a public benefit corporation, though the technology described herein is unrelated to that role.

that O-Man released more slowly from K_2 hydrogels *in vitro* than R-Man. *In vivo*, the clearance of O-Man from K_2 hydrogels was slower than O-Man alone. We attributed the slower release rate to the formation of dynamic imine bonds between reactive aldehyde groups on O-Man and the lysine residues on K_2. This imine interaction was also observed to improve K_2 + O-Man hydrogel strength and shear recovery without significantly influencing secondary structure or peptide nanofiber formation. There were no observed differences in the *in vivo* release rates of O-Man loaded in K_2, R-Man loaded in K_2, and R-Man alone. These data suggest that, after subcutaneous injection, R-Man naturally persists longer *in vivo* than O-Man and minimally interacts with the peptide hydrogel. These results highlight a potentially critical, but previously unreported, difference in the *in vivo* behavior of O-Man and R-Man and demonstrate that K_2 can be used to normalize the release of O-Man to that of R-Man. Further, since K_2 itself is an adjuvant, a combination of O-Man and K_2 could be used to enhance the immunostimulatory effects of O-Man for applications such as infectious disease vaccines and cancer immunotherapy.

Graphical Abstract

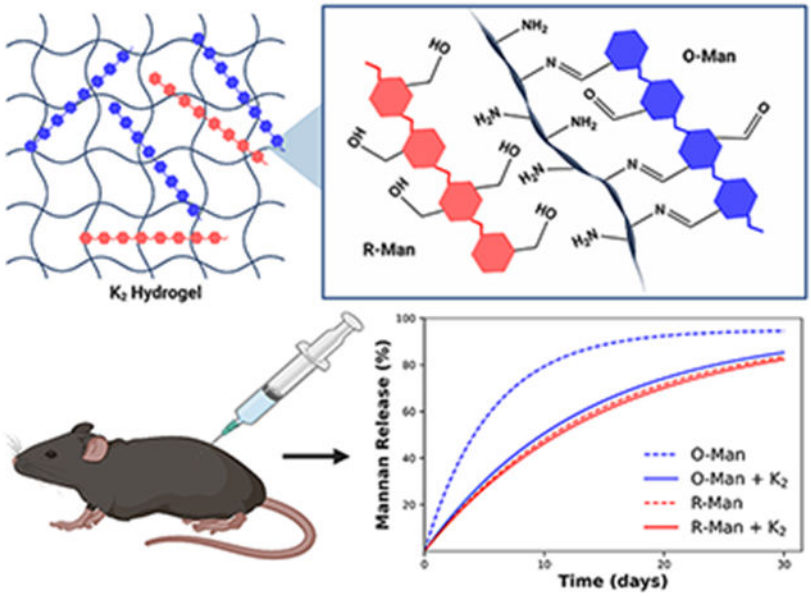

INTRODUCTION

Linear β-(1–4) Mannan is a water-soluble and biodegradable polysaccharide produced by many plants and fungi.[1] Due to its ability to stimulate the immune system by interacting with pattern recognition receptors on the surface of innate immune cells, mannan has gained interest as an adjuvant for vaccines and cancer immunotherapies.[2–4] Adjuvants can improve the effectiveness of immunotherapies and vaccines by activating antigen-presenting cells (APCs), improving antigen uptake by APCs, extending the duration of the immune response, controlling antigen delivery, and directing the adaptive immune response.[2] Mannan acts as an APC-targeting agent that significantly enhances the immunological response to antigens and elicits a stronger immune response than its corresponding monomer, mannose.[5,6]

Mannan is often used in either its oxidized or reduced form to allow for bioconjugation, and both reduced mannan (R-Man) and oxidized mannan (O-Man) bioconjugates have been used in a variety of immunomodulatory applications.[5,7] The oxidation of mannan results in the formation of reactive aldehyde groups that alter key chemical and biological properties of the polysaccharide.[8–10] The presence of aldehydes on mannan allows for chemical modification through the formation of imine, oxime, and hydrazone bonds, along with others.[11] These mannan bioconjugates can be used in their oxidized form or can be reduced after conjugation, converting aldehydes to hydroxyl groups, to prevent further reactivity. For example, peptide epitopes of myelin basic protein have been conjugated to R-Man to decrease the proliferation of autoreactive T cells and ameliorate symptoms of multiple sclerosis.[12,13] O-Man, on the other hand, has been conjugated to Mucin 1 for cancer immunotherapy applications to promote cellular immunity to tumor cells and prevent adenocarcinoma reoccurrence.[14,15] Conversely, the combination of Mucin 1 and R-Man lead to a poor immunological response with no substantial formation of cellular immunity, demonstrating the differing biological responses to R-Man and O-Man.[16] These two forms of mannan can be purposefully used to leverage their specific functional properties and control the type of immune response generated. It has been observed that the conjugation of antigens to O-Man primarily induces Th1 immune responses, associated with the induction of cytotoxic $CD8^+$ T cells, while antigen conjugation to R-Man results in predominantly Th2 B cell-mediated antibody immune responses.[17] Despite these differing chemical and biological properties, little attention has been paid to the *in vivo* residence times of O- and R-Man or their optimal delivery for maximal therapeutic and/or prophylactic efficacy.

Many clinical immunotherapies and prophylactics require repeated, high-dose administration which can compromise patient safety, compliance, and efficacy.[18] The frequent administration of high doses of immunomodulatory materials can lead to chronic inflammation, autoimmunity, hypersensitivity, and/or organ failure.[19–22] Thus, mannan-based immunomodulation, like many other immunotherapeutics and prophylactics, may benefit from a controlled-release delivery system to overcome these challenges through dose sparing and avoiding the need for frequent material administration.[23] Injectable hydrogels represent one potentially attractive mannan delivery system due to their ability to locally deliver therapeutic agents over extended periods of time following minimally invasive administration. A wide variety of materials have been used to form injectable hydrogels, leveraging mechanisms such as supramolecular self-assembly, in situ cross-linking, or sol–gel transitions under physiological temperature or pH.[24–26] Several research groups have engineered systems that combine the use of mannan and injectable hydrogels,[27–29] but the controlled release of mannan and the differing release properties of oxidized and reduced mannan have been largely unexplored.

Peptide-based hydrogels are of clinical interest due to their modular bioactivity, ability to control the release of a variety of payloads, and shear thinning and self-healing properties that allow for injection through small-bore needles.[29,30] Injectable peptide hydrogels have been used in a variety of immunotherapeutic and infectious disease applications[31–33] and have been previously combined with carbohydrates to make supramolecular materials that mimic the extracellular matrix.[34,35] Self-assembling peptide hydrogels have also shown

promise as immunotherapeutic agents for cancer and infectious disease due to their ability to act as adjuvants and to control the release of immunomodulating payloads.[36–39]

Multidomain peptides (MDPs) are a class of self-assembling peptides that use a sequence of alternating polar and nonpolar residues flanked by charged residues to favor β-sheet formation while providing the molecular frustration necessary to form a self-supporting fibrous hydrogel.[40] These hydrogels are of particular interest due to their biocompatibility, shear recovery, and drug delivery capabilities.[41] Their possible immunotherapy applications are bolstered by their modular amino acid building blocks, which allow for diverse chemical functionality that has been shown to influence host immune responses,[42] including the preferential induction of humoral immunity.[43] Composite delivery systems are of particular interest for combination cancer immunotherapy where several immunomodulatory agents delivered together can synergize to enhance treatment efficacy,[44] and MDP hydrogels have been shown to have broad utility for the delivery of many therapeutic payloads. For example, previous investigations have used MDPs to modulate the delivery of proteins, small molecules, and liposomes *in vitro* and *in vivo*.[43,45–48] The ability of MDP hydrogels to control the release of carbohydrate payloads, however, has not been explored. MDPs have typically leveraged complementary electrostatic interactions or hydrophobic interactions to control the payload release rate. These interactions, however, may be insufficient for many payloads, like mannan, that are hydrophilic and uncharged under physiological conditions. Additionally, no previous study has employed dynamic covalent interactions to tune release kinetics from MDP hydrogels.

In the current study, we investigated the ability of a lysinerich MDP hydrogel, Ac–$K_2(SL)_6K_2$–Am (referred to as K_2), to control the release of oxidized and reduced mannan *in vitro* and *in vivo*. K_2 was first designed in 2009,[41] and it has become one of the most widely studied MDPs for small molecule and protein delivery.[43,46,48] We hypothesized that the aldehydes on O-Man would react with the primary amines on the four lysine side chains of K_2, forming reversible covalent imine bonds that would slow the release of O-Man but not R-Man, which lacks aldehyde groups (Figure 1). Dynamic imine bonds have been previously exploited for the controlled release of therapeutic payloads from biomaterials, bioconjugation of carbohydrates to proteins and peptides, and the development of shear-thinning carbohydrate-based hydrogels.[49–52] By leveraging this imine interaction, we found that K_2 significantly extends the release of oxidized mannan relative to reduced mannan *in vitro* and can prolong the release of O-Man but not R-Man—which lacks the ability to form dynamic imine bonds—*in vivo*.

RESULTS AND DISCUSSION

Aldehyde Quantification.

O-Man and R-Man were prepared from native mannan purified by alkaline extraction from *Saccharomyces cerevisiae*. Initial oxidation by propidium iodide produced O-Man, which was subsequently reduced under mild conditions with excess ammonia borane to yield R-Man (Figure 2A). The successful synthesis of both R-Man and O-Man was confirmed through a fluorometric aldehyde detection assay to determine the percent of oxidized mannose monomers, referred to as aldehyde functionalization (Figure 2B). Size

exclusion chromatography demonstrated that the reaction resulted in minimal changes to carbohydrate size; however, a new low molecular weight peak did emerge as a result of oxidation/reduction (Figure S1). O-Man was found to have an average aldehyde functionalization of 17 ± 4% while R-Man fell below the limit of quantification for the assay (0.12%), thus confirming successful reduction. To investigate if imine bond formation occurred between amines in K_2 and the aldehyde groups on O-Man, the aldehyde functionalization of a solution of 0.09 wt % K_2 and 0.01 wt % O-Man—a 10-fold lower concentration of the peptide used in subsequent experiments to avoid hydrogel formation—was quantified. This solution contains an approximately 11-fold molar excess (see Experimental Section) of primary amines on the peptide to aldehydes on the oxidized carbohydrate. Mixing K_2 and O-Man led to a significant decrease in aldehyde functionalization compared to O-Man alone, suggesting that 65 ± 5% of the aldehydes on O-Man had been consumed in imine bond formation with K_2.

Secondary Structure and TEM Characterization.

To ensure that the inclusion of mannan did not disrupt peptide secondary structure or fiber formation, both O-Man and R-Man were loaded into K_2, and the resulting hydrogels were characterized by Fourier transform infrared spectroscopy (FTIR), circular dichroism spectroscopy (CD), and transmission electron microscopy (TEM). As seen in the IR spectra, K_2 loaded with O-Man, K_2 loaded with R-Man, and K_2 alone all exhibited an amide I peak around 1620 cm^{-1}, indicative of β-sheet structure (Figure 3A). The smaller peak 1695 cm^{-1} present in all the spectra suggest the presence of antiparallel β-sheets,[53] which is expected from previous reports of K_2.[42] We hypothesized that the slight differences in peak shape around 1620 cm^{-1} in K_2 loaded with O-Man may be due to changes in secondary structure upon the addition of O-Man. Thus, CD was employed to further assess the secondary structure of these hydrogel-forming materials in solution. As seen in the CD spectra (Figure 3B), all three exhibit a maximum at 198 nm and a minimum at 218 nm, characteristic signals of β-sheet secondary structure. Taken together, these results suggest that the addition of O-Man or R-Man into K_2 does not perturb β-sheet formation. Therefore, the shift in the amide I peak of O-Man loaded into K_2 is circumstantially attributed to the presence of imine bonds, which are expected to have an FTIR peak around 1630 cm^{-1} from C=N stretching.[54] To confirm that this shift in the FTIR spectrum of K_2 loaded with O-man is due to imine bond formation, the amide I region peaks of the MDP E_2 (Ac-EE(SL)$_6$EE-Am) loaded with R-Man and O-Man were evaluated. The E_2 peptide hydrogel contains glutamate residues instead of lysine residues and is thus devoid of primary amines and cannot form imine bonds with the oxidized carbohydrate. The spectra of E_2 with O-Man and R-Man are nearly identical and there is no observed shift in the amide I peak of E_2 loaded with O-Man, further supporting that this shift in the amide I FTIR peak of K_2 loaded with O-Man is due to imine bonding (Figure S2).

Although these spectroscopic techniques confirm the presence of secondary structure in all the peptide formulations and imine bonding between O-Man and K_2, these methods are unable to report on nanoscale peptide morphology. To confirm that the incorporation of R-Man or O-Man did not interfere with nanofiber formation, K_2 loaded with O-Man or R-Man were imaged using negative-stain TEM. TEM images of both K_2 loaded with

O-Man (Figure 3C) and K_2 loaded with R-Man (Figure 3D) confirm the presence of an extensive nanofiber network similar to what has been previously reported in K_2.[55] The slight differences in the appearance of the two samples is likely an artifact from negative stain TEM sample preparation. Additional TEM images of R-Man are included in the Supporting Information (Figure S3).

Rheological Properties.

We hypothesized that the dynamic covalent imine bonds formed between O-Man and the lysine residues on the K_2 peptide would cross-link the fibrous peptide network, thus strengthening the hydrogel and accelerating its shear recovery. Oscillatory rheology was used to investigate the storage (G') and loss (G'') moduli as well as the shear recovery of all three hydrogels to study their viscoelastic properties. All materials tested behaved as largely frequency-independent viscoelastic hydrogels as indicated by $G' > G''$ at all oscillatory frequencies tested (Figure S4). K_2 loaded with O-Man had the highest G' of 460 ± 42 Pa followed by K_2 loaded with R-Man (G' = 290 ± 40 Pa). K_2 loaded with unmodified mannan (Man) and K_2 alone had the lowest G' values at 140 ± 3 and 75 ± 4 Pa, respectively (Figure 4A). These data confirmed that the imine bonds between O-Man and K_2 serve to cross-link hydrogel fibers and strengthen the hydrogel. The significant increase in G' of K_2 loaded with R-Man compared to K_2 alone and K_2 loaded with unmodified mannan was unexpected, as there are undetectable concentrations of aldehydes in R-Man, and as such, imine cross-linking cannot occur. Thus, the increase in hydrogel strength observed when R-Man is loaded into K_2 compared to when Man is loaded into K_2 appears to be the consequence of a different interaction between the processed carbohydrate and the peptide. As shown in Figure 1A, the oxidation and subsequent reduction of mannan results in the ring opening of mannose monomers, referred to as a “hinged” carbohydrate. It is known that naturally stiff carbohydrates increase in flexibility as a consequence of ring opening oxidation.[56,57] Thus, the observed increase in G' upon the addition of R-Man may be a consequence of this increase in carbohydrate flexibility.

Shear recovery is an important property of supramolecular hydrogels for biomedical applications because it allows them to behave as a liquid in the syringe during injection before rapidly reforming as a hydrogel *in situ*. K_2 loaded with O-Man recovered 88 ± 3% of its predeformation storage modulus within 10 min of being subjected to 200% strain for 1 min. K_2 loaded with R-Man and unloaded K_2 demonstrated statistically similar percent recoveries, 74 ± 1% and 69 ± 2%, respectively. K_2 loaded with unmodified mannan had the lowest shear recovery of 57 ± 6% (Figure 3B), again indicating that processing mannan changes its chemical properties and the way it interacts with the peptide. The significantly higher shear recovery in O-Man-loaded K_2 compared to all other groups is likely due to the dynamic imine bonds assisting in hydrogel recovery after deformation, which has been previously reported for imine-cross-linked hydrogels.[50] The improved shear recovery in K_2 when loaded with R-Man compared to K_2 loaded with mannan may again be attributed to the increased flexibility of the hinged carbohydrate. This theory is further supported by the observation that the inclusion of stiffer, unmodified mannan into the hydrogel significantly reduces shear recovery compared to the unloaded K_2 hydrogel. To confirm that the rheological differences between K_2 loaded with R-Man and O-Man are due

to imine bonding, the rheological properties of E_2 loaded with the two carbohydrates was characterized. There were no significant differences in G' or the shear recovery between O-Man and R-Man loaded E_2 (Figure S5). These results suggest that the differences in rheological properties between K_2 loaded with O-Man and K_2 loaded with R-Man are due to imine bond formation.

In Vitro and *In Vivo* Release.

The *in vitro* release rates of unmodified mannan (Man), O-Man, and R-Man from K_2 were determined using a fluorescence-based *in vitro* equilibrium release assay using a custom 3D-printed 48-well plate setup described in detail in the Experimental Section (Figure S6). K_2 loaded with O-Man and K_2 loaded with R-Man demonstrated statistically similar initial burst release rates which may be due to the release of mannan on the surface of each hydrogel. However, the long-term release rate of K_2 loaded with R-Man was significantly higher than the long-term release rate of O-Man from K_2. Unmodified mannan loaded in K_2 had the highest equilibrium release of 99 ± 2.3% by hour 24 of the assay. The significantly more rapid release of the unmodified carbohydrate may be due to differences in rheological properties and/or the increased stiffness of the unoxidized/reduced carbohydrate. This result also supports the hypothesis that the hinged carbohydrate allows for more physical entanglement with the hydrogel compared to the stiff native carbohydrate. At the end of 24 h, only 45 ± 1.4% of O-Man had been released from K_2 compared to 68 ± 0.5% for R-Man with each material appearing to approach an equilibrium between mannan in the hydrogel and supernatant (Figure 5A). The delay in O-Man release could be due to dynamic covalent imine interactions between O-Man and the hydrogel, whereas R-Man, which could not covalently interact with K_2, released more quickly. Alternatively, these variations in release rates could be caused by differences in the rheological properties of the two hydrogels, as seen in the case of unmodified mannan loaded in K_2. To provide further support for the hypothesis that *in vitro* release kinetics are imine bond-mediated, the equilibrium release profiles of O-Man and R-Man from the MDP E_2, which lacks primary amines and cannot form imine bonds. As expected, the release rates of O-Man and R-Man from E_2 were not significantly different from each other, which supports the conclusion that the delay in O-Man *in vitro* release from K_2 is due to imine bonding (Figure S7). Like in the case of K_2, unmodified mannan was more rapidly released from E_2 than the O-Man and R-Man, demonstrating that this result is likely due to the nature of the unmodified carbohydrate and not the chemical functionality of the peptide hydrogel. Thus, these results support the hypothesis that imine interactions between O-Man and K_2 can be used to modulate O-Man release.

The release rates of soluble and K_2-loaded O-Man and R-Man *in vivo* were assessed using a fluorescence-based release assay performed in hairless SKH1-Elite mice. Mannan clearance was observed through the steady decrease in fluorescent signal at the site of injection over the 56-day monitoring period (Figure 5B). The first 30 days are graphed in Figure 5C to focus on the most dynamic portion of the release curves. The release profiles of all the materials tested demonstrated first-order release kinetics and fit well ($R^2 \geq 0.90$) to a one-phase decay exponential equation that is described in more detail in the Experimental Section (eq 1 and Figure S8). Soluble O-Man released at a significantly faster rate (0.18

days^{-1}) than soluble R-Man (0.07 days^{-1}), and the half-life of O-Man (3.9 days) was found to be less than half that of R-Man (9.7 days) (Table 1). These data suggest there is a significant inherent difference in the retention times of R-Man and O-Man *in vivo* ($p < 0.0001$).

As hypothesized, O-Man loaded in K_2 hydrogels demonstrated slower clearance than unloaded O-Man. Loading O-Man into K_2 resulted in an over 2-fold increase in the half-life, indicating that the imine interaction can be leveraged to substantially prolong O-Man release *in vivo* (Table 1). In contrast with our *in vitro* results, however, R-Man and O-Man were released from K_2 hydrogels at a similar rate. Additionally, R-Man cleared from the injection site at the same rate regardless of if it was loaded into K_2 or not, suggesting that the hydrogel plays a minimal role in dictating the release of R-Man *in vivo*. The different observed release rates of O-Man and R-Man emphasize the dominant role that the chemical functionality of the carbohydrate plays on the *in vivo* retention of mannan, which has not been previously explored.

The discrepancy between our *in vivo* and *in vitro* results highlights the inability of *in vitro* release assays to adequately model the *in vivo* environment. Many other studies investigating supramolecular hydrogel drug delivery have seen similar discrepancies between *in vitro* and *in vivo* release kinetics.[43,58,59] The results of the current study and these related investigations demonstrate that the complex biological environment (complete with proteins, cells, etc.) plays a large role in governing the release kinetics from supramolecular materials. New *in vitro* release assays are needed in the field of drug delivery to better mimic the *in vivo* environment environment and more accurately predict *in vivo* release kinetics. Despite the limitations of the assay, the difference between the *in vitro* and *in vivo* release results in the current study suggests that innate slower clearance of R-Man *in vivo* can compensate for its lack of imine interactions with K_2.

Interestingly, the clearance rates of R-Man, R-Man-loaded K_2, and O-Man-loaded K_2 are all similar demonstrated by the fact that all their mean half-lives and rate constants reside within their 95% confidence intervals based on *in vivo* release data (Table 1). There are two seemingly likely explanations for the observed results. First, O-Man could be covalently trapped in the hydrogel by the formation of imine bonds causing a delay in the release from the injection site. Second, O-Man's rapid dissipation from the injection site could be due to some currently unidentified aldehyde-mediated clearance mechanism. Thus, O-Man's imine bond formation with K_2 quenches the reactive aldehyde groups on O-Man, preventing its aldehyde-mediated clearance and slowing its *in vivo* release rate to that of R-Man. This explanation suggests that primary amines and not the hydrogel itself are necessary to prolong the release of O-Man *in vivo*, so the same or a similar effect on the release rate should be observed when O-Man is mixed with just soluble primary amines.

To test this hypothesis, fluorescently labeled O-Man was mixed with glycine, at equimolar concentrations to primary amines in the K_2 hydrogel samples, to quench the reactive aldehydes, and then were administered to mice. Over the course of 30 days, O-Man with glycine pretreatment behaved very similarly to O-Man on its own, demonstrating that the hydrogel is necessary to delay oxidized carbohydrate release (Figure S9). This result, in

combination with *in vitro* release results, suggests that the mechanism underlying this delayed release is due to local carbohydrate entrapment in the hydrogel via the formation of imine bonds. The observed differences between O-Man mixed with glycine and K_2 may be explained by the dynamic covalent bonding polyvalency of the carbohydrate and the hydrogel. Since the peptide hydrogel has many attachment sites to the carbohydrate, for O-Man to be cleared, the hydrogel needs to degrade or every attachment site between K_2 and the carbohydrate needs to break. In the case of glycine-bound O-Man, we hypothesize that the imine bonds with glycine can be exchanged with a primary amine on protein at a single site, and this is sufficient to allow for clearance as no other imine attachment is anchoring the carbohydrate in place as is the case with the hydrogel. Since the hydrogel itself is responsible for the observed improvement in O-Man *in vivo* persistence, the release rate of O-Man may be tunable by changing the concentration of the hydrogel or doping in MDPs that lack free amines to alter the number of imine bonds formed. In this study, we demonstrate that K_2 can be used to delay the release of O-Man alone. Using this approach, however, future investigations may be able to use K_2 as a composite delivery system to control the release of O-Man and other immunomodulatory compounds simultaneously, and thereby improving the efficacy of mannan-based immunotherapeutics and prophylactics.

CONCLUSION

Despite growing interest in using mannan in biomedical applications, there is a dearth of research into the *in vivo* retention of O-Man and R-Man. Temporal control of other adjuvants and immunotherapeutic payloads has previously been shown to significantly improve prophylactic and treatment efficacy.[60–63] It is likely that mannan release kinetics play a key role in the immune response generated by mannan conjugates as well, but this area of research remains largely unexplored. Recent investigations have found that the efficacy of immunotherapies employing mannan is strongly influenced by *in vivo* dynamics, including the persistence of constituent immunostimulatory agents,[60,64] and thus the ability to manipulate mannan kinetics may be useful for optimizing therapeutic outcomes. In the current study, we demonstrate for the first time that O-Man has an intrinsically faster *in vivo* clearance than R-Man, and that the K_2 MDP hydrogel can be used to delay the release of a carbohydrate payload. The accelerated clearance of O-Man can be ameliorated by loading it into K_2 hydrogels whose abundance of amines reacts with aldehydes on O-Man to form imine bonds. We show that the inclusion of R-Man and O-Man into K_2 does not interfere with peptide nanofiber self-assembly or hydrogel formation. The imine cross-links between O-Man and K_2 also lead to a significant improvement in hydrogel strength and shear recovery.

The timing of mannan delivery, previously achieved by altering dosing regimens, has been shown to be particularly important for combination immunotherapies.[65] We demonstrate here that temporal control of O-Man can be achieved without requiring multiple doses by using the K_2 hydrogel. The results of the current study also open the possibility of designing MDP-based composite delivery systems that include O-Man conjugates with other MDP-compatible immunomodulatory payloads (e.g., antibodies, protein subunits, small molecule adjuvants) for combination immunotherapy or vaccine development. Further, these results imply that K_2 may be able to act as a platform for the controlled delivery

of a variety of oxidized carbohydrates and potentially other aldehyde-containing payloads, including small molecules. To the best of our knowledge, previous investigations into the immunomodulatory effects of mannan conjugates have not considered differences in *in vivo* release or investigated potential controlled-release systems that modulate temporal presentation. Thus, the results from the current study may shed light on the previously reported immunological differences between R-Man and O-Man and help guide future research into translational mannan-based bioconjugates and biomaterials.

EXPERIMENTAL PROCEDURES

Solid-Phase Peptide Synthesis.

Peptides were synthesized manually using standard Fluorenylmethyloxycarbonyl (Fmoc)-based chemistry. Resin and Fmoc-protected amino acids were supplied by Novabiochem (MilliporeSigma, Burlington, MA). Fmoc-protected low-loading MBHA rink-amide resin (1 equiv) was deprotected with two steps of excess 25% v/v piperidine in DMF:DMSO 1:1 for 5 min each. All Fmoc deprotection steps were performed identically and checked using the ninhydrin test for primary amines. Coupling was achieved with the addition of preactivated Fmoc-protected amino acids (4 equiv), hexafluorophosphate azabenzotriazole tetramethyl uronium (3.95 equiv) and N,N-diisopropylethylaine (DIEA) (6 equiv) to the resin in a minimal amount of DMF:DMSO 1:1 for 20 min at RT. The process was repeated until the peptide was complete. N-terminal acetylation was performed with the addition of acetic anhydride (200 equiv) and DIEA (75 equiv) in DCM two times for 45 min. Peptides were cleaved from the resin by reacting it with a cleavage cocktail composed of trifluoroacetic acid:Anisole:triisopropylethylsilane:ethylenedithiol:H_2O 90:2.5:2.5:2.5:2.5 for 3 h at RT. The cleavage cocktail was then evaporated off to approximately 1 mL with a nitrogen stream and peptide was triturated with cold diethyl ether.

HPLC Purification.

All peptides were purified by high-performance liquid chromatography (HPLC) on an XBridge Protein BEH C4 OBD Prep column (Waters Corporation, Milford, MA) using two different solvent systems. For K_2, a solvent system of Milli-Q water with 0.05% trifluoracetic acid (solvent A) and acetonitrile with 0.05% trifluoroacetic acid (solvent B) was used for purification. E_2 was purified using Milli-Q water supplemented with 4 mM acetic acid and 5 mM ammonium hydroxide (solvent A) and acetonitrile with the same buffer (solvent B). Peptide solutions (10 mg/mL) were injected on the column in a volume of 1 mL 80% solvent A and 20% solvent B. Purification was achieved using a 3% solvent B/min gradient from 5% to 50% solvent B while monitoring the absorbance at 220 and 280 nm on a UV detector. Sample purity was confirmed by ultraperformance liquid chromatography (UPLC) using the same HPLC solvents and matrix assisted laser desorption/ionization mass spectrometry (MALDI MS) (Figures S10 and S11).

Mannan Preparation.

Mannan purified by alkaline extraction (MilliporeSigma, Burlington, MA) was labeled with aminooxy-functionalized Cy647 (Biotium, Fremont, CA) using the standard protocol from the supplier with minor modifications. Mannan was dissolved at 100 μM (1 equiv) in

1× PBS, 100 mM sodium acetate, and 150 mM sodium chloride. The carbohydrate was oxidized by adding propidium iodide to a final concentration of 10 mM (100 equiv) and incubating for 10 min at RT. Oxidation was stopped with the addition of ethylene glycol to a concentration of 100 mM (1000 equiv). Aminooxy-functionalized Cy647 (5 equiv) was then reacted with aldehyde groups on the O-Man for 2 h with 1× aniline buffer (Biotium, Fremont, CA) as a catalyst. The carbohydrate was purified with an Amicron Ultra-15 3 kDa cutoff spin filter (MilliporeSigma, Burlington, MA) to yield labeled O-Man. R-Man was prepared by reducing O-Man with a final concentration of 10 mM (100 equiv) ammonia borane overnight with agitation and the product was purified using a 3 kDa spin filter. Ammonia-borane was employed because it is a gentle reducing agent that can be used for the selective reduction of aldehydes and keytones,[66] and thus would preserve the integrity of the conjugated fluorophore. All materials were lyophilized and stored at −20 °C until use. Unlabeled O-Man and R-Man were prepared using the same method as above without the addition of fluorophore.

Fluorophore-labeled unmodified (not oxidized or reduced) mannan (Man) was prepared by using amine-reactive TFP-AZdye 647 (Click Chemistry Tools, Scottsdale, AZ) to react with trace amount of mannoprotein that has been used previously to make mannan-protein bioconjugates without oxidation or reduction.[49] In brief, mannan (10 mg/mL) was labeled with 10 equiv of AZdye 647 overnight in pH 8.2 0.2 M sodium bicarbonate buffer. The resulting solution was purified using a PD-10 desalting column (Cytiva, Marlborough, MA) and lyophilized until used.

Size Exclusion Chromatography.

Size exclusion chromatography was performed using a HiLoad 16/600 Superdex 200 prep grade column (Cytiva, Marlborough, MA) on an Agilent 1290 Infinity 2 HPLC system (Santa Clara, CA). Unmodified and reduced mannan (not fluorophore-labeled) were dissolved in 1 mL and injected onto the column with a flow rate of 1 mL/min in PBS. The absorbance was measured at 210 nm over 150 min. Chromatograms were area normalized and background subtracted for comparison.

Hydrogel Preparation.

Mannan-containing hydrogels were prepared by making two separate 2 wt.% solutions of peptide and carbohydrate. The solutions were then mixed in a 9:1 peptide:carbohydrate ratio. The volume was then doubled with 1× HBSS to make a final solution of 0.9 wt.% peptide and 0.1 wt.% carbohydrate. Hydrogel without mannan was made in the same way but without the addition of mannan. The solutions were then incubated at RT overnight to allow for complete hydrogelation.

Aldehyde Quantification.

The number of aldehyde groups per mg of mannan was measured using a fluorometric aldehyde quantification assay kit (MilliporeSigma, Burlington, MA) following the standard protocol from the supplier. If brief, 0.1 mg/mL of oxidized and reduced mannan and 0.1 mg/mL oxidized mannan with 0.9 mg/mL K_2 were prepared in Milli-Q H_2O. After overnight incubation at RT, 50 μL of each solution was added in triplicate to a Costar black flat-bottom

96-well plate (Corning Inc., Corning, NY) along with aldehyde standards. Master reaction mix (50 μL) was added to each well and incubated at RT in the dark for 30 min with orbital shaking. To develop the assay, 25 μL of reaction buffer was added to each well, and the fluorescence was measured immediately (Ex/Em 365/435 nm) using a microplate reader (Tecan, Mannedorf, Switzerland). The aldehyde functionalization percentage was calculated using the aldehyde standard curve to determine the molar concentration of aldehyde in each well. This value was divided by two to account for the fact that two aldehydes are generated per mannose monomer oxidation. The final functionalization percentage was determined by then dividing half the molar concentration of aldehydes by the molar concentration of mannose monomer in solution.

Fourier Transform Infrared Spectroscopy.

Grazing angle FTIR spectra were obtained using a NicoletTM iS20 FTIR spectrometer (Thermo Fisher Scientific, Waltham, MA). The instrument was purged with nitrogen to avoid capturing signals from atmospheric molecular vibrations. Hydrogel samples, prepared as previously described, were plated (10 μL) and dried with a stream of nitrogen until all water had evaporated. Absorbance spectra were collected as an accumulation of 30 measurements and background subtracted. The amide I FTIR peak was visualized by plotting the area normalized absorbance from 1575 to 1705 cm^{-1}.

Circular Dichroism Spectroscopy.

Circular dichroism spectroscopy was performed on a Jasco J-810 spectropolarimeter with temperature control. Hydrogel samples, prepared as previously described, were loaded into a quartz cuvette with a path length of 0.1 mm and analyzed at RT. Wavelength scans were performed between 190 and 250 nm, and spectra were collected as the average of 5 accumulations. The molar residue ellipticity (MRE) was calculated using the equation $[\theta] = \theta/(c \times l \times nr)$, where θ is ellipticity in mdeg, c is the concentration in mmol/L, l is path length of the cuvette in mm, and nr is the number of amino acid residues in the peptide.

Transmission Electron Microscopy.

Negative staining of peptide hydrogel fibers was performed using 2% (w/v) phosphotungstic acid (PTA) in fresh Milli-Q water. Samples were prepared with the syringe-filtered PTA solution. Briefly, a 300CF-Cu film was stained with a 0.05% (w/v) solution of peptide and mannan. The peptide solution was allowed to sit on the carbon side of the film for 60 s, and then the excess solution was wicked away. Subsequently, 50 μL of PTA solution was allowed to sit on the film for 5 min before removing the excess solution as well. Micrographs were taken on a JEOL JEM 2100F electron microscope at 120 kV.

Rheology.

Oscillatory rheology measurements were collected using an AR-G2 rheometer (TA Instruments, New Castle, DE). Rheology was performed on 75 μL samples transferred to the instrument with a truncated 200 μL pipet to minimize shear. Samples were equilibrated at 1 rad/s and 1% strain for 30 min. The final hydrogel strength was determined by obtaining the storage (G') and loss (G'') moduli at the end of this period. After equilibration, a

frequency sweep was performed over the range of 0.1–10 rad/s at a constant 1% strain. Shear recovery experiments were conducted after the frequency sweep by allowing the hydrogel to equilibrate for 2 min at 1 rad/s and 1% strain and then sheared for 1 min at 200% strain. Recovery was then monitored for 10 min at the starting conditions, and the percent recovery was calculated by comparing the final G' and G'' values at the end of the 10 min to the values at the end of the initial 2 min equilibration.

In Vitro Release Assays.

Hydrogels were prepared with 10% fluorescent R-Man or O-Man the day before the assay and hydrogelation proceeded at RT in the dark overnight. Hydrogels were then plated (50 μL) into a custom 3D-printed 48-well plate in a depression on the left side of each well with a truncated pipet tip. The wells of the custom 48-well plate are printed on a Form 3+ 3D printer using PU Rigid 650 resin (Formlabs, Somerville, MA) by converting two laterally adjacent wells on a 96-well plate into a single oblong well with the same positions, so they are compatible with a microplate reader.[43] The hydrogels were then plated on the left side of the well and then allowed to rest for 5 min to reform as hydrogels before supernatant (400 μL) was then added to each well (Figure S6). The supernatant used was 1× PBS with 4.5 mM glucose. Solutions that mimicked 100% release were prepared in the same way as the hydrogels but without peptide. The assay was then placed in a microplate reader (Tecan, Mannedorf, Switzerland) set to 37 °C with orbital shaking (142 rpm), and time points were taken every 45 min by reading the fluorescence on the right side of each well (opposite end of where the hydrogel was plated). The percent release was calculated by dividing the fluorescent intensity of each sample by the intensity of the 100% release solution at each time point.

In Vivo Release Assays.

All animal studies were conducted in accordance with a protocol approved by the Rice University Institutional Animal Care and Use Committee (IACUC-20-065-RU) in the Animal Resource Facility at Rice University. SKH1-Elite mice were first obtained from Charles River Laboratories (Wilmington, MA) and allowed to acclimate. The day before injection, hydrogels were prepared as described above with 100% fluorescent mannan. Gly+O-Man samples were prepared with 1.5 mg/mL glycine to match the concentration of free amines in the K_2 hydrogel. Samples (50 μL) were loaded into insulin syringes and stored at 4 °C overnight. Immediately before administering the injections, the background tissue autofluorescence (Ex/Em 640/700 nm) of each mouse was acquired using an In Vivo Imaging System (IVIS) small animal imager (PerkinElmer, Waltham, MA). Background autofluorescence was subtracted from all subsequent measurements. Samples were then injected bilaterally subcutaneously into the rear flank and imaged at several time points until the fluorescence was no longer discernible from the background. Release was calculated by drawing equally sized rectangular regions of interest around the injection site and dividing the observed total radiant efficiency in that region by the maximum total radiant efficiency observed on the first day of the experiment. The entirety of the *in vivo* release data was then fit to a first-order release model with the initial value set to 0% and the plateau set to 95% (eq 1) in GraphPad Prism 9 using a least-squares regression. The plateau was set based on the maximum release observed for O-Man, which never surpassed 95% during the time

period monitored (Figure S8). The half-lives and rate constants of the resulting first-order release models were reported with their 95% confidence intervals.

$$y = -95e^{-k \cdot x} + 95 \quad (1)$$

Statistics.

The same two statistical analyses were performed for all experiments. Single group comparisons were compared by unpaired *t* test. Multiple group comparisons were calculated by one-way ANOVA with Tukey's multiple comparisons test. Calculations were performed in GraphPad Prism 9. Statistical significance is denoted with asterisks as follows: $*p < 0.05$; $**p < 0.01$; $***p < 0.001$; $****p < 0.0001$. Error bars and reported error represents one standard deviation from the mean unless otherwise specified.

Supplementary Material

Refer to Web version on PubMed Central for supplementary material.

ACKNOWLEDGMENTS

The authors would like to thank Mei-Li Laracuente and Tyler Graf for assistance with data collection and Marina Yu for assistance with designing the table of contents figure. This work was supported in full (100%) by public funding. B.H.P. and C.C.C. were supported by the National Science Foundation Graduate Research Fellowship Program. This work was supported by the National Institutes of Health Grants R03EB031495, K22AI146215, R01DE021798, and R01DE030140. The table of contents figure and Figure 1 were made using BioRender.com.

REFERENCES

(1). Moreira LRS; Filho EXF An Overview of Mannan Structure and Mannan-Degrading Enzyme Systems. Appl. Microbiol. Biotechnol 2008, 79 (2), 165–178. [PubMed: 18385995]

(2). Wu Z; Liu K Overview of Vaccine Adjuvants. Med. Drug Discovery 2021, 11, 100103.

(3). Hu H-G; Li Y-M Emerging Adjuvants for Cancer Immunotherapy. Front. Chem 2020, 8, 1. [PubMed: 32117862]

(4). Pogostin BH; McHugh KJ Novel Vaccine Adjuvants as Key Tools for Improving Pandemic Preparedness. Bioengineering 2021, 8 (11), 155. [PubMed: 34821721]

(5). Bashiri S; Koirala P; Toth I; Skwarczynski M Carbohydrate Immune Adjuvants in Subunit Vaccines. Pharmaceutics 2020, 12 (10), 965. [PubMed: 33066594]

(6). François-Heude M; Méndez-Ardoy A; Cendret V; Lafite P; Daniellou R; Ortiz Mellet C; García Fernández JM; Moreau V; Djedaïni-Pilard F Synthesis of High-Mannose Oligosaccharide Analogues through Click Chemistry: True Functional Mimics of Their Natural Counterparts against Lectins? Chem. Weinh. Bergstr. Ger 2015, 21 (5), 1978–1991.

(7). Matsoukas J; Deraos G; Kelaidonis K; Hossain MK; Feehan J; Tzakos AG; Matsoukas E; Topoglidis E; Apostolopoulos V Myelin Peptide–Mannan Conjugate Multiple Sclerosis Vaccines: Conjugation Efficacy and Stability of Vaccine Ingredient. Vaccines 2021, 9 (12), 1456. [PubMed: 34960201]

(8). Benito-Villalvilla C; Soria I; Subiza JL; Palomares O Novel Vaccines Targeting Dendritic Cells by Coupling Allergoids to Mannan. Allergo J. Int 2018, 27 (8), 256–262. [PubMed: 30546997]

(9). Shibuya N; Goldstein IJ; Van Damme EJ; Peumans WJ Binding Properties of a Mannose-Specific Lectin from the Snowdrop (Galanthus Nivalis) Bulb. J. Biol. Chem 1988, 263 (2), 728–734. [PubMed: 3335522]

(10). Misaki A; Kakuta M; Meah Y; Goldstein IJ Purification and Characterization of the α-1,3-Mannosylmannose-Recognizing Lectin of Crocus VernusBulbs *. J. Biol. Chem 1997, 272 (41), 25455–25461. [PubMed: 9325257]

(11). Kölmel DK; Kool ET Oximes and Hydrazones in Bioconjugation: Mechanism and Catalysis. Chem. Rev 2017, 117 (15), 10358–10376. [PubMed: 28640998]

(12). Katsara M; Yuriev E; Ramsland PA; Tselios T; Deraos G; Lourbopoulos A; Grigoriadis N; Matsoukas J; Apostolopoulos V Altered Peptide Ligands of Myelin Basic Protein (MBP87–99) Conjugated to Reduced Mannan Modulate Immune Responses in Mice. Immunology 2009, 128 (4), 521–533. [PubMed: 19930042]

(13). Matsoukas JM; Ligielli I; Chasapis CT; Kelaidonis K; Apostolopoulos V; Mavromoustakos T Novel Approaches in the Immunotherapy of Multiple Sclerosis: Cyclization of Myelin Epitope Peptides and Conjugation with Mannan. Brain Sci. 2021, 11 (12), 1583. [PubMed: 34942885]

(14). Apostolopoulos V; Pietersz GA; Tsibanis A; Tsikkinis A; Drakaki H; Loveland BE; Piddlesden SJ; Plebanski M; Pouniotis DS; Alexis MN; et al. Pilot Phase III Immunotherapy Study in Early-Stage Breast Cancer Patients Using Oxidized Mannan-MUC1 [ISRCTN71711835]. Breast Cancer Res. BCR 2006, 8 (3), R27. [PubMed: 16776849]

(15). Vassilaros S; Tsibanis A; Tsikkinis A; Pietersz GA; McKenzie IFC; Apostolopoulos V Up to 15-Year Clinical Follow-up of a Pilot Phase III Immunotherapy Study in Stage II Breast Cancer Patients Using Oxidized Mannan-MUC1. Immunotherapy 2013, 5 (11), 1177–1182. [PubMed: 24188672]

(16). Apostolopoulos V; Pietersz GA; Loveland BE; Sandrin MS; McKenzie IF Oxidative/Reductive Conjugation of Mannan to Antigen Selects for T1 or T2 Immune Responses. Proc. Natl. Acad. Sci. U. S. A 1995, 92 (22), 10128–10132. [PubMed: 7479739]

(17). Tang CK; Lodding J; Minigo G; Pouniotis DS; Plebanski M; Scholzen A; McKenzie IFC; Pietersz GA; Apostolopoulos V Mannan-Mediated Gene Delivery for Cancer Immunotherapy. Immunology 2007, 120 (3), 325–335. [PubMed: 17328786]

(18). Xiao Q; Li X; Li Y; Wu Z; Xu C; Chen Z; He W Biological Drug and Drug Delivery-Mediated Immunotherapy. Acta Pharm. Sin. B 2021, 11 (4), 941–960. [PubMed: 33996408]

(19). Zhao Z; Zheng L; Chen W; Weng W; Song J; Ji J Delivery Strategies of Cancer Immunotherapy: Recent Advances and Future Perspectives. J. Hematol. Oncol. J. Hematol Oncol 2019, 12 (1), 126. [PubMed: 31779642]

(20). June CH; Warshauer JT; Bluestone JA Is Autoimmunity the Achilles' Heel of Cancer Immunotherapy? Nat. Med 2017, 23 (5), 540–547. [PubMed: 28475571]

(21). Riley RS; June CH; Langer R; Mitchell MJ Delivery Technologies for Cancer Immunotherapy. Nat. Rev. Drug Discovery 2019, 18 (3), 175–196. [PubMed: 30622344]

(22). Abbas M; Moussa M; Akel H Type I Hypersensitivity Reaction. In StatPearls; StatPearls Publishing: Treasure Island (FL), 2022.

(23). Carter P Improving the Efficacy of Antibody-Based Cancer Therapies. Nat. Rev. Cancer 2001, 1 (2), 118–129. [PubMed: 11905803]

(24). Huynh CT; Nguyen MK; Lee DS Injectable Block Copolymer Hydrogels: Achievements and Future Challenges for Biomedical Applications. Macromolecules 2011, 44 (17), 6629–6636.

(25). Overstreet DJ; Dutta D; Stabenfeldt SE; Vernon BL Injectable Hydrogels. J. Polym. Sci., Part B: Polym. Phys 2012, 50 (13), 881–903.

(26). Nguyen MK; Lee DS Injectable Biodegradable Hydrogels. Macromol. Biosci 2010, 10 (6), 563–579. [PubMed: 20196065]

(27). Wu Q; Gong C; Shi S; Wang Y; Huang M; Yang L; Zhao X; Wei Y; Qian Z Mannan Loaded Biodegradable and Injectable Thermosensitive PCL-PEG-PCL Hydrogel for Vaccine Delivery. Soft Mater. 2012, 10 (4), 472–486.

(28). He T; Liang X; Li L; Gong S; Li X; Zhang M; Zhu S; Xiao H; Wu Q; Gong C A Spontaneously Formed and Self-Adjuvanted Hydrogel Vaccine Triggers Strong Immune Responses. Mater. Des 2021, 197, 109232.

(29). Kim S; Lee J; Im S; Kim WJ Injectable Immunogel Based on Polymerized Phenylboronic Acid and Mannan for Cancer Immunotherapy. J. Control. Release Off. J. Control. Release Soc 2022, 345, 138–146.

(30). Chakraborty P; Guterman T; Adadi N; Yadid M; Brosh T; Adler-Abramovich L; Dvir T; Gazit E A Self-Healing, All-Organic, Conducting, Composite Peptide Hydrogel as Pressure Sensor and Electrogenic Cell Soft Substrate. ACS Nano 2019, 13 (1), 163–175. [PubMed: 30588802]

(31). Dasgupta A; Hassan Mondal J; Das D Peptide Hydrogels. RSC Adv. 2013, 3 (24), 9117–9149.

(32). Xing R; Li S; Zhang N; Shen G; Möhwald H; Yan X Self-Assembled Injectable Peptide Hydrogels Capable of Triggering Antitumor Immune Response. Biomacromolecules 2017, 18 (11), 3514–3523. [PubMed: 28721731]

(33). Si Y; Tian Q; Zhao F; Kelly SH; Shores LS; Camacho DF; Sperling AI; Andrade MS; Collier JH; Chong AS Adjuvant-Free Nanofiber Vaccine Induces in Situ Lung Dendritic Cell Activation and TH17 Responses. Sci. Adv 2020, 6 (32), eaba0995. [PubMed: 32821819]

(34). Soares da Costa D; Brito A; Reis RL; Pashkuleva ISupramolecular Assemblies of Glycopeptides as Mimics of the Extracellular Matrix. In Multifunctional Hydrogels for Biomedical Applications; John Wiley & Sons, Ltd, 2022; pp 149–159. DOI: 10.1002/9783527825820.ch7.

(35). Brito A; Abul-Haija YM; da Costa DS; Novoa-Carballal R; Reis RL; Ulijn RV; Pires RA; Pashkuleva I Minimalistic Supramolecular Proteoglycan Mimics by Co-Assembly of Aromatic Peptide and Carbohydrate Amphiphiles. Chem. Sci 2019, 10 (8), 2385–2390. [PubMed: 30881666]

(36). Liu J; Zhang L; Yang Z; Zhao X Controlled Release of Paclitaxel from a Self-Assembling Peptide Hydrogel Formed in Situ and Antitumor Study in Vitro. Int. J. Nanomedicine 2011, 6, 2143–2153. [PubMed: 22114478]

(37). Sun Z; Song C; Wang C; Hu Y; Wu J Hydrogel-Based Controlled Drug Delivery for Cancer Treatment: A Review. Mol. Pharmaceutics 2020, 17 (2), 373–391.

(38). Luo Z; Wu Q; Yang C; Wang H; He T; Wang Y; Wang Z; Chen H; Li X; Gong C; et al. A Powerful CD8+ T-Cell Stimulating D-Tetra-Peptide Hydrogel as a Very Promising Vaccine Adjuvant. Adv. Mater 2017, 29 (5), 1601776.

(39). Huang H; Shi J; Laskin J; Liu Z; McVey DS; Sun XS Design of a Shear-Thinning Recoverable Peptide Hydrogel from Native Sequences and Application for Influenza H1N1 Vaccine Adjuvant. Soft Matter 2011, 7 (19), 8905–8912.

(40). Moore AN; Hartgerink JD Self-Assembling Multidomain Peptide Nanofibers for Delivery of Bioactive Molecules and Tissue Regeneration. Acc. Chem. Res 2017, 50, 714–722. [PubMed: 28191928]

(41). Aulisa L; Dong H; Hartgerink JD Self-Assembly of Multidomain Peptides: Sequence Variation Allows Control over Cross-Linking and Viscoelasticity. Biomacromolecules 2009, 10 (9), 2694–2698. [PubMed: 19705838]

(42). Lopez-Silva TL; Leach DG; Azares A; Li I-C; Woodside DG; Hartgerink JD Chemical Functionality of Multidomain Peptide Hydrogels Governs Early Host Immune Response. Biomaterials 2020, 231, 119667. [PubMed: 31855625]

(43). Pogostin BH; Yu MH; Azares AR; Euliano EM; Lai CS; Saenz G; Wu SX; Farsheed AC; Melhorn SM; Graf TP; et al. Multidomain Peptide Hydrogel Adjuvants Elicit Strong Bias towards Humoral Immunity. Biomater. Sci 2022, 10 (21), 6217–6229. [PubMed: 36102692]

(44). Ott PA; Hodi FS; Kaufman HL; Wigginton JM; Wolchok JD Combination Immunotherapy: A Road Map. J. Immunother. Cancer 2017, 5 (1), 16. [PubMed: 28239469]

(45). Li I-C; Moore AN; Hartgerink JD Missing Tooth" Multidomain Peptide Nanofibers for Delivery of Small Molecule Drugs. Biomacromolecules 2016, 17 (6), 2087–2095. [PubMed: 27253735]

(46). Leach DG; Dharmaraj N; Piotrowski SL; Lopez-Silva TL; Lei YL; Sikora AG; Young S; Hartgerink JD STINGel: Controlled Release of a Cyclic Dinucleotide for Enhanced Cancer Immunotherapy. Biomaterials 2018, 163, 67–75. [PubMed: 29454236]

(47). Wickremasinghe NC; Kumar VA; Hartgerink JD Two-Step Self-Assembly of Liposome-Multidomain Peptide Nanofiber Hydrogel for Time-Controlled Release. Biomacromolecules 2014, 15 (10), 3587–3595. [PubMed: 25308335]

(48). Kumar VA; Shi S; Wang BK; Li I-C; Jalan AA; Sarkar B; Wickremasinghe NC; Hartgerink JD Drug-Triggered and Cross-Linked Self-Assembling Nanofibrous Hydrogels. J. Am. Chem. Soc 2015, 137 (14), 4823–4830. [PubMed: 25831137]

(49). Lang S; Huang X Carbohydrate Conjugates in Vaccine Developments. Front. Chem 2020, 8, 284. [PubMed: 32351942]

(50). Li S; Pei M; Wan T; Yang H; Gu S; Tao Y; Liu X; Zhou Y; Xu W; Xiao P Self-Healing Hyaluronic Acid Hydrogels Based on Dynamic Schiff Base Linkages as Biomaterials. Carbohydr. Polym 2020, 250, 116922. [PubMed: 33049836]

(51). Yu R; Petit E; Barboiu M; Li S; Sun W; Chen C Biobased Dynamic Hydrogels by Reversible Imine Bonding for Controlled Release of Thymopentin. Mater. Sci. Eng., C 2021, 127, 112210.

(52). Hu X; Jazani AM; Oh JK Recent Advances in Development of Imine-Based Acid-Degradable Polymeric Nanoassemblies for Intracellular Drug Delivery. Polymer 2021, 230, 124024.

(53). Nabedryk E; Garavito RM; Breton J The Orientation of Beta-Sheets in Porin. A Polarized Fourier Transform Infrared Spectroscopic Investigation. Biophys. J 1988, 53 (5), 671–676. [PubMed: 2455547]

(54). Namli H; Turhan O Background Defining during the Imine Formation Reaction in FT-IR Liquid Cell. Spectrochim. Acta. A. Mol. Biomol. Spectrosc 2006, 64 (1), 93–100. [PubMed: 16095956]

(55). Moore AN; Hartgerink JD Self-Assembling Multidomain Peptide Nanofibers for Delivery of Bioactive Molecules and Tissue Regeneration. Acc. Chem. Res 2017, 50 (4), 714–722. [PubMed: 28191928]

(56). Smidsrød O; Painter T Effect of Periodate Oxidation upon the Stiffness of the Alginate Molecule in Solution. Carbohydr. Res 1973, 26 (1), 125–132.

(57). Kristiansen KA; Potthast A; Christensen BE Periodate Oxidation of Polysaccharides for Modification of Chemical and Physical Properties. Carbohydr. Res 2010, 345 (10), 1264–1271. [PubMed: 20227684]

(58). Braegelman AS; Ollier RC; Su B; Addonizio CJ; Zou L; Cole SL; Webber MJ Macromolecular Solute Transport in Supramolecular Hydrogels Spanning Dynamic to Quasi-Static States. ACS Appl. Bio Mater 2022, 5 (10), 4589–4598.

(59). Liang G; Yang Z; Zhang R; Li L; Fan Y; Kuang Y; Gao Y; Wang T; Lu WW; Xu B Supramolecular Hydrogel of a D-Amino Acid Dipeptide for Controlled Drug Release in Vivo. Langmuir 2009, 25 (15), 8419–8422. [PubMed: 20050040]

(60). Roth GA; Saouaf OM; Smith AAA; Gale EC; Hernández MA; Idoyaga J; Appel EA Prolonged Codelivery of Hemagglutinin and a TLR7/8 Agonist in a Supramolecular Polymer–Nanoparticle Hydrogel Enhances Potency and Breadth of Influenza Vaccination. ACS Biomater. Sci. Eng 2021, 7 (5), 1889–1899. [PubMed: 33404236]

(61). Chen N; Johnson MM; Caollier MA; Gallovic MD; Bachelder EM; Ainslie KM. Tunable Degradation of Acetalated Dextran Microparticles Enables Controlled Vaccine Adjuvant and Antigen Delivery to Modulate Adaptive Immune Responses. J. Controlled Release 2018, 273, 147–159.

(62). Roth GA; Picece VCTM; Ou BS; Luo W; Pulendran B; Appel EA. Designing Spatial and Temporal Control of Vaccine Responses. Nat. Rev. Mater 2022, 7 (3), 174–195. [PubMed: 34603749]

(63). Jin Q; Liu Z; Chen Q. Controlled Release of Immunotherapeutics for Enhanced Cancer Immunotherapy after Local Delivery. J. Controlled Release 2021, 329, 882–893.

(64). Ou BS; Saouaf OM; Baillet J; Appel EA Sustained Delivery Approaches to Improving Adaptive Immune Responses. Adv. Drug Delivery Rev 2022, 187, 114401.

(65). Caisová V; Uher O; Nedbalová P; Jochmanová I; Kvardová K; Masáková K; Krejčová G; Pad'ouková L; Chmelař J; Kopecký J; et al. Effective Cancer Immunotherapy Based on Combination of TLR Agonists with Stimulation of Phagocytosis. Int. Immunopharmacol 2018, 59, 86–96. [PubMed: 29635103]

(66). Shi L; Liu Y, Liu Q; Wei B; Zhang G. Selective Reduction of Aldehydes and Ketones to Alcohols with Ammonia Borane in Neat Water. Green Chem. 2012, 14 (5), 1372–1375.

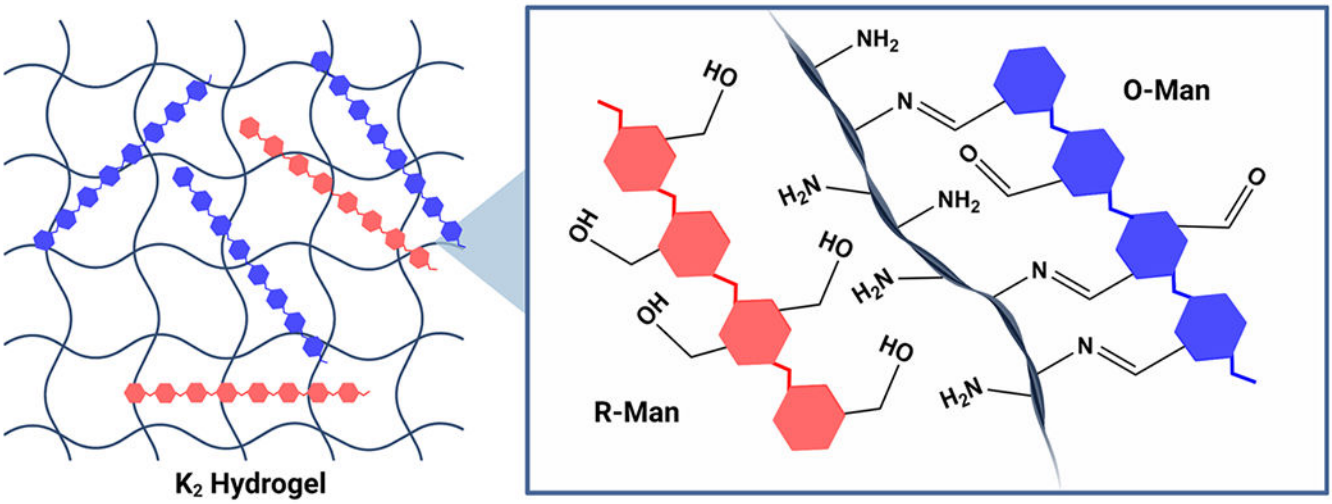

Figure 1.

Schematic showing O-Man (blue) and R-Man (red) loaded into a K_2 hydrogel. Aldehyde groups on O-Man can form imine bonds with the amines on the K_2 peptide fibers whereas the hydroxyl groups present on R-Man cannot form imine bonds with K_2.

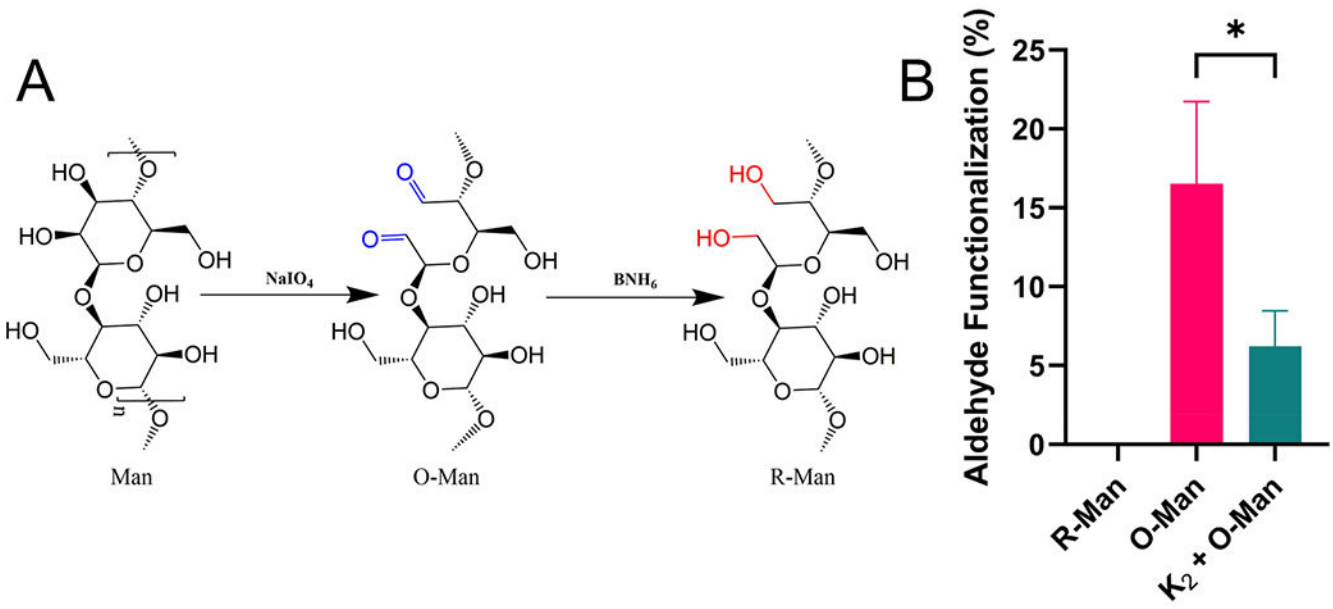

Figure 2.

(A) Schematic of oxidation and reduction reactions on a representative portion of the linear mannan polysaccharide showing one mannose monomer being oxidized and then subsequently reduced. (B) Results of the fluorometric aldehyde quantification assay show the percent of mannose monomers oxidized, referred to as aldehyde functionalization, for O-Man and R-Man. Mixing O-Man with K_2 led to a significant decrease in aldehyde content, suggesting the formation of imine bonds between the peptide and the carbohydrate.

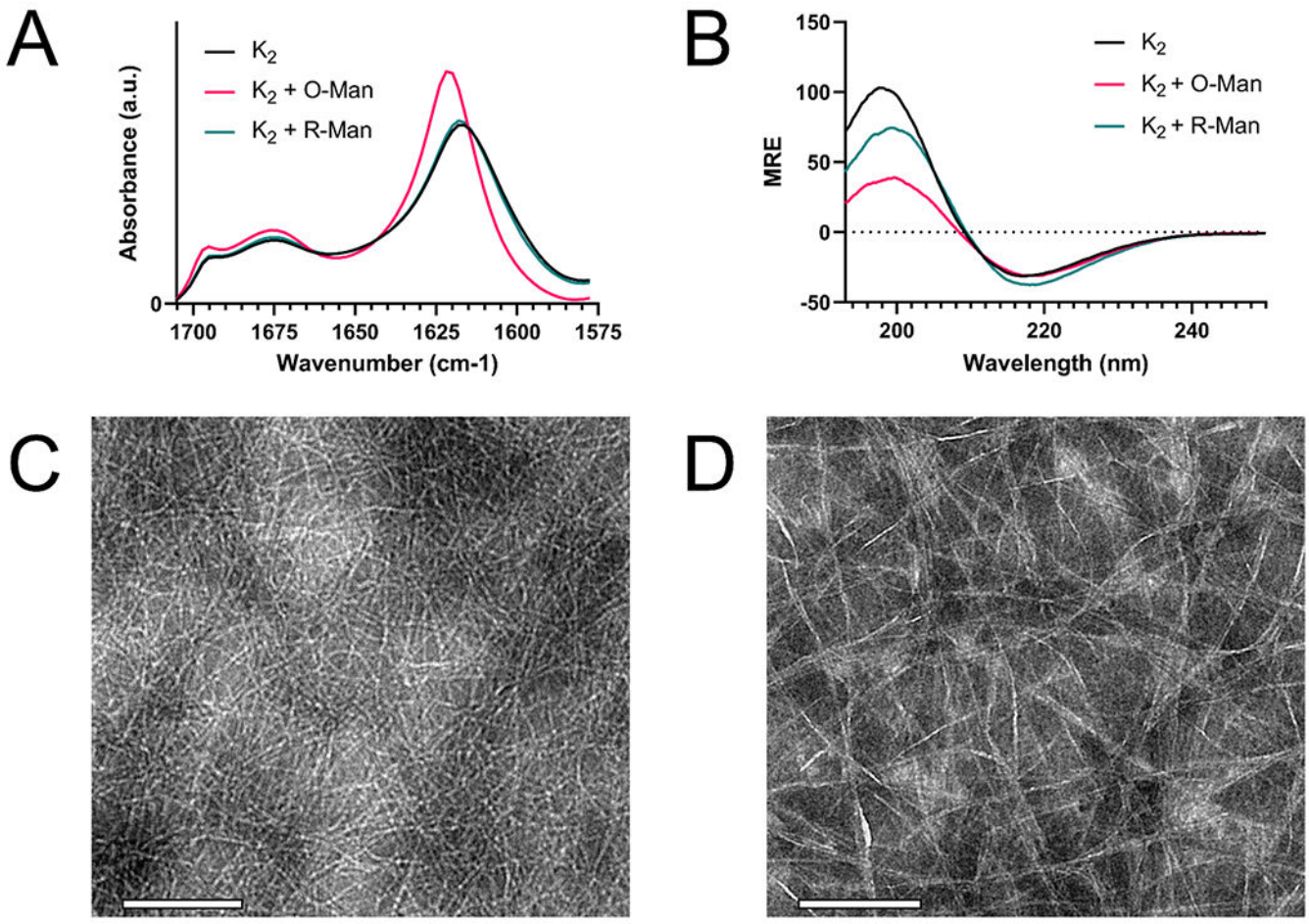

Figure 3.

Structural characterization of K_2 loaded with O-Man and R-Man. (A) Area normalized FTIR absorbance spectrum of K_2, K_2 loaded with O-Man (K_2 + O-Man), and K_2 loaded with R-Man (K_2 + R-Man) showing characteristic peaks for antiparallel sheet: 1675 cm^{-1}, 1695 cm^{-1}, and β-sheet: 1620 cm^{-1}. The peak shift observed in K_2 + O-Man is attributed to the presence of imine bonds. (B) CD spectrum of K_2, K_2 + O-Man, and K_2 + R-Man show a characteristic minimum at 218 nm and maximum at 198 nm for β-sheets. TEM negative stain of (C) K_2 + O-Man and (D) K_2 + R-Man demonstrate both have a nanofibrous architecture. The scale bar is 200 nm.

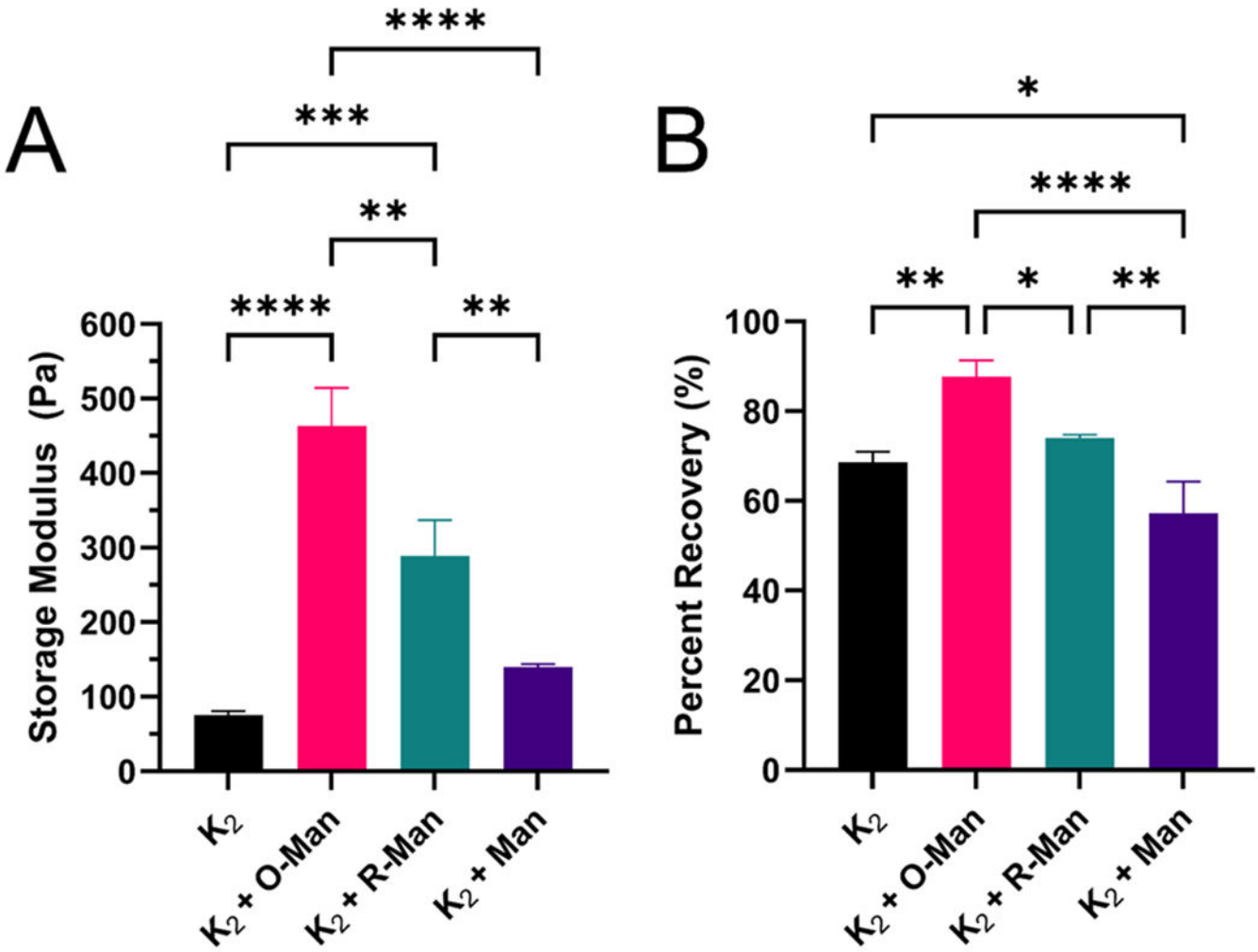

Figure 4.

Oscillatory rheology characterization of the viscoelastic properties of K_2, K_2 loaded with O-Man (K_2 + O-Man), K_2 loaded with O-Man (K_2 + R-Man), and K_2 loaded with mannan (K_2 + Man). (A) Storage modulus of each hydrogel and (B) percent recovery 10 min after a deformation force yielding 200% strain.

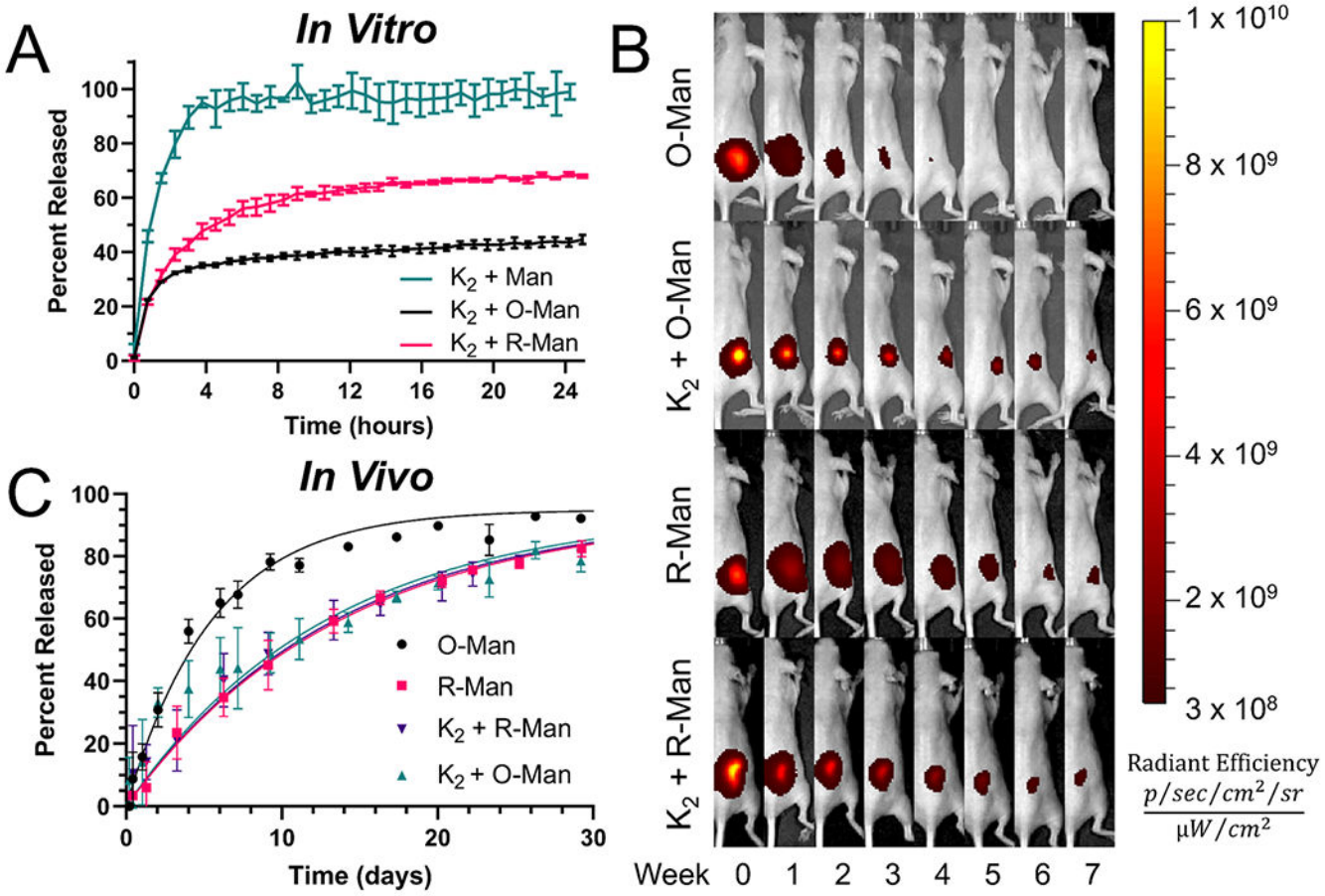

Figure 5.

(A) *In vitro* release of K_2 loaded with unmodified mannan (K_2 + Man), O-Man (K_2 + O-Man), and R-Man (K_2 + R-Man) over a 24 h period demonstrates an overall slower release of K_2 + O-Man. (B) *In vivo* release IVIS images of O-Man, R-Man, K_2 + O-Man, and K_2 + R-Man for 56 days after injection. (C) Graph of the percent of released carbohydrate from the first 30 days of the *in vivo* release experiment (n = 4–5). R-Man, K_2 + O-Man, and K_2 + R-Man all release at similar rates while O-Man is cleared from the site of injection at a significantly faster rate.

Table 1.

In Vivo Mannan Release Rate Parameters[a]

Sample	R^2	$t_{1/2}$ (days)	k (days^{-1})
O-Man	0.98	3.9 ± 0.2	0.18 ± 0.01
R-Man	0.98	9.7 ± 0.4	0.07 ± 0.01
K_2 + R-Man	0.94	9.4 ± 0.6	0.07 ± 0.01
K_2 + O-Man	0.90	9.0 ± 0.8	0.08 ± 0.01

[a]Rate constants (k) and halt-lives ($t_{1/2}$) ± 95% confidence interval extracted by fitting all release data over the 56-day period to a first-order one-phase decay equation (Experimental Sectioneq 1). These models adequately fit the data in all cases ($R^2 \geq 0.9$).